High-resolution three-dimensional optical coherence tomography imaging of kidney microanatomy *ex vivo*

Yu Chen
Massachusetts Institute of Technology
Department of Electrical Engineering and
    Computer Science
Research Laboratory of Electronics
Cambridge, Massachusetts 02139

Peter M. Andrews
Georgetown University Medical Center
Department of Biochemistry, Molecular and
    Cellular Biology
Washington, DC 20007

Aaron D. Aguirre
Massachusetts Institute of Technology
Department of Electrical Engineering and
    Computer Science
Research Laboratory of Electronics
Cambridge, Massachusetts 02139

Joseph M. Schmitt
LightLab Imaging
Westford, Massachusetts 01886

James G. Fujimoto
Massachusetts Institute of Technology
Department of Electrical Engineering and
    Computer Science
Research Laboratory of Electronics
Cambridge, Massachusetts 02139

Abstract. Optical coherence tomography (OCT) is an emerging medical imaging technology that enables high-resolution, noninvasive, cross-sectional imaging of microstructure in biological tissues *in situ* and in real time. When combined with small-diameter catheters or needle probes, OCT offers a practical tool for the minimally invasive imaging of living tissue morphology. We evaluate the ability of OCT to image normal kidneys and discriminate pathological changes in kidney structure. Both control and experimental preserved rat kidneys were examined *ex vivo* by using a high-resolution OCT imaging system equipped with a laser light source at 1.3-μm wavelength. This system has a resolution of 3.3 μm (depth) by 6 μm (transverse). OCT imaging produced cross-sectional and *en face* images that revealed the sizes and shapes of the uriniferous tubules and renal corpuscles. OCT data revealed significant changes in the uriniferous tubules of kidneys preserved following an ischemic or toxic (i.e., mercuric chloride) insult. OCT data was also rendered to produce informative three-dimensional (3-D) images of uriniferous tubules and renal corpuscles. The foregoing observations suggest that OCT can be a useful non-excisional, real-time modality for imaging pathological changes in donor kidney morphology prior to transplantation. © *2007 Society of Photo-Optical Instrumentation Engineers.* [DOI: 10.1117/1.2736421]

1 Introduction

Optical coherence tomography (OCT) is an emerging technology that can generate high-resolution images of tissues *in situ* and in real time.[1] OCT is analogous to ultrasound imaging, except that it uses the echo delay of light instead of sound to generate images. By employing broadband optical light sources, axial resolutions of 1 to 2 μm can be achieved by OCT,[2] which is more than an order of magnitude above that obtainable for high-frequency ultrasound.[3] Therefore, OCT has the potential of providing high-resolution, noninvasive images of architectural morphology in organs and tissues. This potential has been demonstrated in a wide range of applications such as ophthalmology,[4–6] cardiology,[7,8] gastroenterology,[9–11] dermatology,[12] dentistry,[13] urology,[14] and gynecology.[15]

To date, there have been no OCT investigations attempting to distinguish the uriniferous tubules and glomeruli of the kidney. In this study, we explore the feasibility and evaluate the capability of high-resolution OCT technology to image normal kidneys, as well as kidneys that had been subjected to an ischemic or a toxic insult. OCT imaging may prove especially important for the kidney because excisional biopsies can produce artifacts that are difficult to distinguish from ischemic and other insults.[16] Also, excisional biopsies are invasive and damaging, and they sample only a very small region of the kidney.

Our observations indicate that OCT can provide valuable morphological information about the uriniferous tubules and renal corpuscles. Since histopathological images of the superficial uriniferous tubules can be used to predict the status of donor kidneys prior to their transplantation,[17] we propose that OCT imaging might be a useful, nonexcisional, and quick procedure for evaluating the status of donor kidneys prior to their transplantation.

Address all correspondence to: Yu Chen, Massachusetts Institute of Technology, Department of Electrical Engineering and Computer Science and Research Laboratory of Electronics, Cambridge, MA 02139. E-mail: chen_yu@mit.edu
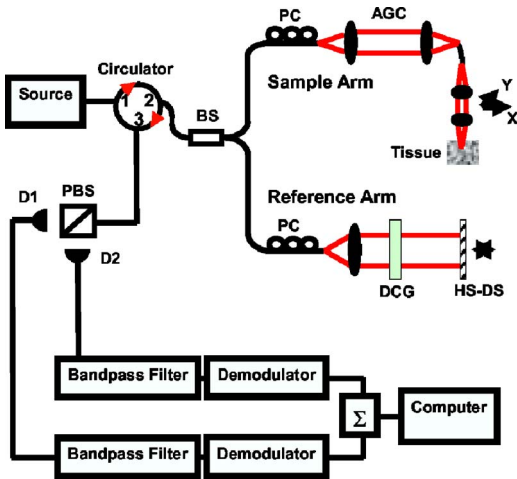
Fig. 1 Schematic of the high-resolution OCT system. BS: 90/10 fiber-based beamsplitter; PC: polarization controller; AGC: air-gap coupling; DCG: dispersion compensating glass; HS-DS: high-speed delay scanner; PBS: polarization beamsplitter; D: detector; Σ: vector summation.

2 Materials and Methods

2.1 Optical Coherence Tomography Imaging

The OCT imaging system used in this study has been described in previous publications.[18] The OCT system was a research prototype based on a commercial OCT system (Lightlab Imaging, Inc., Westford, Massachusetts) that was modified for ultrahigh-resolution performance (Fig. 1). Imaging was performed using a special broadband laser source consisting of a compact femtosecond Cr^{4+}:Forsterite laser combined with nonlinear spectral broadening in a dispersion-shifted fiber to generate a 180-nm bandwidth at a center wavelength of 1260 nm with 50-mW output power. To achieve ultrahigh-resolution imaging performance, the dispersion between the sample and reference arms of the interferometer needs to be carefully matched. Dispersion compensating glasses (SFL6 and LaKN22) were inserted in the reference arm to compensate for the collimating and focusing optics in the sample arm. An air-gap coupling was used in the sample arm to compensate for the air path in the reference arm from the collimator to the scanning delay mirror. An axial resolution of 4.6 μm in air ($\sim$3.3 μm in tissue when scaled by the approximate tissue refractive index of 1.38) was achieved. The average optical power incident on the tissue was $\sim$10 mW. The reference arm power was adjusted to maximize the signal-to-noise ratio (SNR), and the system detection sensitivity was measured to be 102 dB. The OCT signal was divided into two orthogonal polarization channels by a polarizing beamsplitter, and the two detector outputs were digitally demodulated using a digital-signal-processing (DSP) board. A polarization diversity OCT signal was obtained from the square root of the sum of the squared signal intensities from the two polarization channels. The polarization diversity detection minimizes polarization artifacts due to the specimen or motion of the sample arm fiber during scanning. The system used a high-speed scanning delay line that acquires 3,125 axial scans per second. Imaging was performed using a fiber-based collimator combined with a microlens that produced a transverse spot size of 6 μm full width at half maximum (FWHM). The collimator and microlens unit was raster (xy) scanned by two precisely controlled stages (Physik Instrumente GmbH & Co. KG, Karlsruhe, Germany). Individual cross-sectional OCT images (xz) were generated at a rate of 2 frames per second with dimensions 3 mm in length (600 pixels) and 2.5 mm in depth (1,600 pixels). Consecutive OCT images in different planes along the y direction were scanned with 3-μm separation to generate a three-dimensional (3-D) volume. The 3-D OCT data was processed and visualized using a 3-D visualization and volumetric rendering software package (Amira, Mercury Computer Systems, Inc., Berlin, Germany). The software allowed the generation of 3-D volumetric views and *en face* (xy) views.

2.2 Ischemic Model

Studies were performed using male rats of the Munich-Wistar strain. The rats were studied when they reached approximately 8 weeks of age, at which time they had a median weight of approximately 250 grams. The rats were maintained on a standard Purina Rat Chow diet (Ralston Purina Co., St. Louis, Missouri) and *ad lib* water intake. The animals were anesthetized with Inactin (120 mg/kg body weight, ip; ATANA Pharma AG, Konstanz, Germany) and placed on a temperature-regulated table. The animals were turned onto their right side, and a left subcostal flank incision was made to expose the left kidney. A 10-cm length of 3-0 silk ligature was looped around the left renal artery at its juncture with the abdominal aorta. Gentle tension on this loop was enough to occlude blood flow to the left kidney. This setup allowed for easy manipulation of blood flow by applying or releasing tension on the silk loop. The femoral vein was cannulated with polyethylene tubing and attached to a 5-cc syringe mounted in a syringe pump (Sage Instruments, Model 341A, Orion Research Inc., Cambridge, Massachusetts). Using this procedure, we evaluated the effects of 60 min ischemia to the left kidney and the effects of sucrose infusion prior to ischemia.

2.3 Sucrose Experiments

Sucrose infusion provides protection from renal ischemia.[19,20] In these studies, a single bolus of 1.0 ml containing 0.25 gm of sucrose was slowly infused into the femoral vein over a period of 90 s prior to induction of ischemia, as described earlier.

2.4 Mercury Toxicity

Mercury was administered (under light ether anesthesia) to three male rats as a single intravenous injection (via the femoral vein) of 1 mg/kg body weight of mercuric chloride made up in normal sterile saline at a concentration of 1 mg/ml. Forty-eight hours following mercury injection, the rats were anesthetized with Ketamine (60 mg/kg, im), followed by sodium pentobarbital (21 mg/kg/ip), and the kidneys were fixed by vascular perfusion using the procedures previously described[21] and outlined in Sec. 2.5. In a previous study, we have shown that the foregoing treatment regimen results in a significant decline in renal function, as determined by serum creatinine and blood urea nitrogen (i.e., BUN) determinations, and significant damage to the S2 segments of the proximal convoluted tubules.[22]
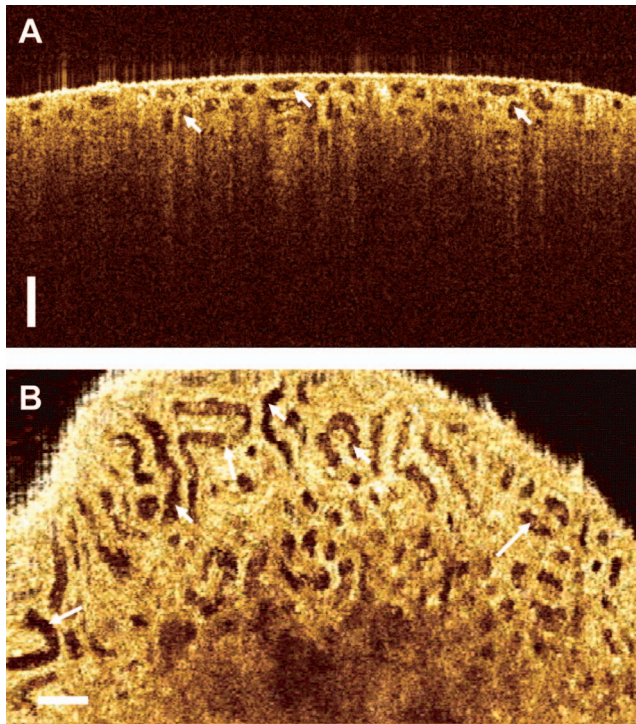
Fig. 2 (a) Two-dimensional OCT image of normal kidney. The open areas represent different cross-sectional planes through the lumens of the uriniferous tubules (arrows). (b) *En face* view of the tubular structure. Bar: 250 μm.

2.5 Preservation of Kidneys for Study

All kidneys (i.e., normal, ischemic, and mercury toxicity models) were preserved *in situ* using a vascular perfusion procedure previously described.[21] Briefly, a loose ligature was placed around the abdominal aorta at a point just above the renal arteries, the inferior vena cava was cut, and a flushing solution consisting of an isotonic phosphate buffer (4.3 g/liter NaH_2PO_4 and 14.8 g/liter NaH_2PO_4) was perfused retrograde through the aorta at a pressure of 140 mm Hg. After the kidneys were cleared of blood (this
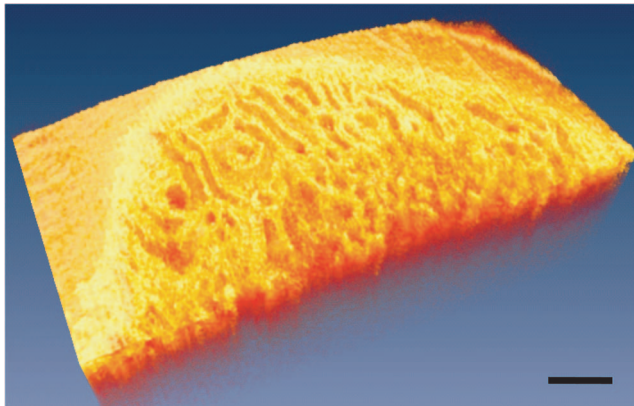

Fig. 3 Three-dimensional reconstruction of OCT cutaway view revealing the contours as well as the winding nature of the superficial uriniferous tubules. Size: 2.0 mm (*L*)×1.0 mm (*W*)×0.7 mm (*D*); cut plane: 150 μm below the top surface.
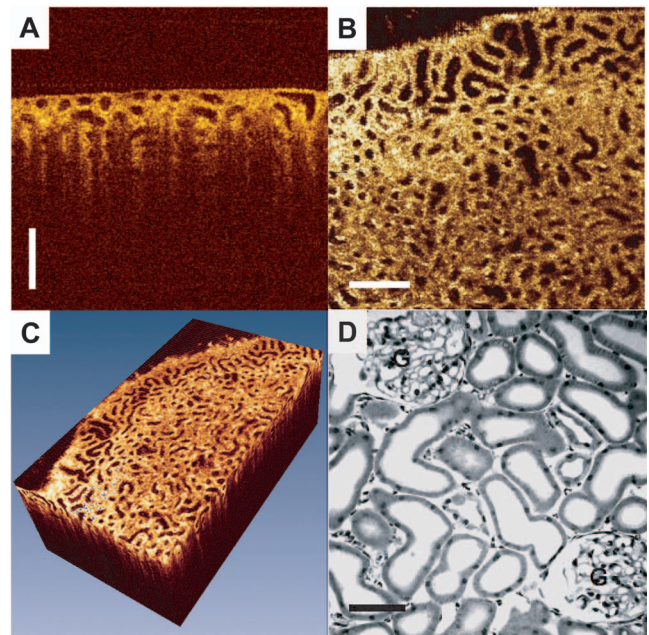

Fig. 4 OCT images of a kidney protected from 1 h of ischemic insult due to prior infusion of sucrose. (a) Cross-sectional image (bar: 250 μm). (b) *En face* image (bar: 250 μm). (c) Three-dimensional view (size: 2.1 mm in length×1.0 mm in width×0.8 mm in height). (d) Plastic-embedded light microscopic section image (bar: 75 μm). G: glomerulus.

occurs within seconds), the abdominal aorta above the level of the renal arteries was tied, and the kidneys were fixed by subsequent vascular perfusion of 2% glutaraldehyde made up in the same phosphate buffer that was used to flush the kidneys. The intact fixed kidneys were removed, and the whole kidneys were placed under the OCT imaging beam and imaged *ex vivo*. After OCT imaging, small tissue blocks from the OCT imaging regions were excised and embedded in JB-4 plus embedding media (Polysciences, Inc., Warrington, Pennsylvania) and sectioned (1 to 2 μm) using a glass knife mounted on a Powertome XL ultramicrotome (Boeckeler Instruments, Inc., Tucson, Arizona). The semithin tissue sections were mounted on glass slides, stained with Multistain (Polysciences, Inc.), and examined and photographed using an Olympus BH-2 light microscope equipped with a Canon digital camera (Model G5 Powershot).

Note: All the animal models, fixation, and euthanasia procedures received prior approval by the Animal Use and Care Committee, Georgetown University Medical Center, in compliance with the Federal Animal Welfare Act.

3 Observations

Using OCT imaging, we were able to obtain cross-sectional images several hundred microns into the kidney parenchyma and to observe cross sections through the uriniferous tubules [Figs. 2(a) and 2(b)]. The uriniferous tubule lumens appeared to be low backscattering (dark region), while the parenchyma appeared to be high backscattering (bright region). An *en face* image can be reconstructed from consecutive cross-sectional images [Fig. 2(b)]. Rendered OCT images using 3-D visualization and volumetric rendering software provided 3-D re-

constructions that revealed the shapes and contours of the winding proximal convoluted tubules (Fig. 3). For comparative purposes, a high-quality, plastic-embedded light microscopic section of this tissue is shown in Fig. 4(d).

There was a significant difference in OCT images between those kidney specimens protected from ischemia by prior infusion of sucrose [Fig. 4(a)–4(c)] and those that received no protection (i.e., no sucrose) prior to the ischemic insult [Fig. 5(a)–5(c)]. The latter (i.e., unprotected kidneys) revealed patches where tubules had lumens either entirely or partially filled with cytoplasmic debris. Although evident in cross-sectional images [Fig. 5(a)], this change was more dramatic when viewed in the *en face* images [Figs. 5(b) and 5(c)]. For comparative purposes, high-quality, plastic-embedded light microscopic sections of normal and ischemic kidneys are seen in Figs. 4(d) and 5(d), respectively. OCT images of kidneys subjected to mercury toxicity revealed regions devoid of tubule lumens due to accumulated cytoplasmic debris and casts. Other tubules exhibit distended lumens due to distal tubule blockage [Fig. 6(a)–6(c)]. Nevertheless, it is difficult to distinguish between the distal and proximal convoluted tubules in these images. The foregoing OCT images correlated with light microscopic images of these kidneys, thereby showing debris in selected proximal convoluted tubules, distal tubule casts, and distended lumens following the mercuric chloride insult [Fig. 6(d)].

Because donor kidneys that are being preserved for possible transplantation are often surrounded by fat and are stored in plastic bags, we evaluated these factors on the ability of the OCT system to image the kidney. Neither translucent plastic wrappings [Fig. 7(a)] nor a layer of superficial fatty connective tissue [Fig. 7(b)] impeded the imaging of several hundred microns into the kidney.

Renal corpuscles containing glomeruli and surrounded by the capsular space of Bowman were also distinguishable in cross-sectional OCT images [Fig. 8(a)]. Three-dimensional processing of these images again provided instructive views of glomerular sizes and shapes, and revealed the space of Bowman between the glomerulus and the parietal epithelium [Fig. 8(b)]. The latter is important because it permits determination of glomerular shrinkage and enlargement, as well as possible attachment to the parietal epithelial capsule. Again, for comparative purposes, a high-quality, plastic-embedded light microscopic section of a superficial renal corpuscle is shown in Fig. 4(d).

4 Discussion

OCT is a rapidly emerging imaging modality that can function as a type of "optical biopsy," thus providing cross-sectional images of tissue architectural morphology *in situ* and in real time.[23] In contrast to standard confocal microscopy, OCT can image with longer working distances and improved penetration depth, without the need for tissue contact. These factors are advantageous for the practical use of this technology in evaluating kidney pathology. While it has been reported that OCT can image up to depths of 1 to 2 mm (Ref. 24), the degree of penetration depends on several factors, including the light-scattering properties of the tissue being analyzed and the confocal parameter of the focusing lens. In this study, we used a relatively high transverse resolution focusing ($6~\mu$m)

in order to have the fine tubule structures (which are about 30 to 40 μm in diam) resolve better; therefore, the depth of field and penetration depth are limited when compared to that of OCT images using 20 to 30 μm spot sizes. We can image up to depths of 300 to 400 μm, which was deep enough to image several layers of the superficial uriniferous tubules and glomeruli. This was also several times deeper than in our previous tandem scanning confocal microscopy (TSCM) study, wherein only the outermost single layer of uriniferous tubules and no glomeruli could be observed.[17] In addition, OCT can provide 3-D images in arbitrary planes[24] and can be performed using a thin flexible endoscope or catheter,[18] or even with a needle,[25] thus enabling ease of use and the possibility of imaging deep within a solid tissue or organ. We should note that OCT had previously been used to image thermal tissue damage to the rat kidney resulting from laser ablation.[26] However, this earlier study focused on the thermal insult site and did not attempt to distinguish components of the renal parenchyma (i.e., uriniferous tubules and glomeruli) as reported here.[26]

Using an ultrahigh-resolution OCT imaging system with a compact broadband Cr^{4+}:Forsterite laser light source, we were able to image the superficial uriniferous tubules and glomeruli of intact, preserved rat kidneys. Using computer rendering software to process these images, we were able to visualize the tubules in different imaging planes and to generate composite 3-D images. The latter proved especially instructive in depicting the shapes, contours, and sizes of the uriniferous tubules and the renal corpuscles. Only scanning electron microscopy of preserved, sectioned, dehydrated, metal-coated samples can provide similar 3-D images.[27]

The 3-D volume rendering enables the visualization of arbitrary planes and subsurface tissue microstructure. The ability to visualize *en face* planes at different depths enables the 3-D tubular organization to be assessed. The 3-D OCT data in this preliminary study is from *ex vivo* samples. This eliminates motion artifacts, since the acquisition speed is limited (2 frames per second). However, with recent advances in OCT imaging technology using spectral/Fourier domain detection, dramatic improvements (~100-fold) in imaging speed are possible.[28–31] These high imaging speeds enable 3-D OCT *in vivo*. In addition, novel microscanning devices such as micromechanical mirror or piezoelectric fiber scanners have been recently developed.[32–34] These advances promise 3-D OCT imaging of kidney structures *in vivo* in the future.

In order to determine the potential usefulness of OCT as a procedure to study kidney pathology, we evaluated kidney samples subjected to ischemia and samples exposed to mercury toxicity. In the ischemic study, some kidneys were protected from the ischemic insult by prior infusion of sucrose. Sucrose is a protective osmotic agent, which prevents cell swelling and rupturing that otherwise would result in damage to the proximal convoluted tubules.[19,20] Areas of proximal convoluted tubules with lumens occluded with debris as a result of 60 min of ischemia were in sharp contrast to samples protected by prior intravenous infusion of sucrose. It is important to note that the correlative light microscopic images of both normal and pathological kidney samples were obtained from kidneys that were fixed *in situ* by vascular perfusion procedures. As noted earlier, vascular perfusion procedures
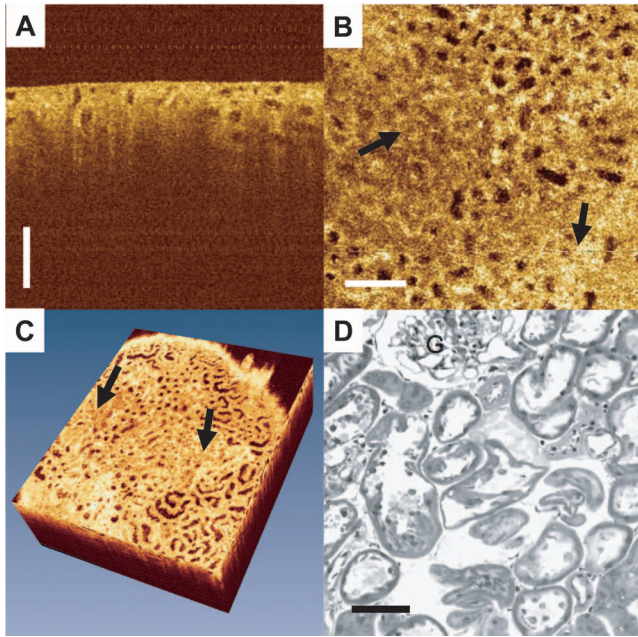
Fig. 5 OCT images of a kidney subjected to 1 h of ischemia followed by 5 min of recovery. (a) Cross-sectional image (bar: 250 μm). (b) *En face* image (bar: 250 μm). (c) Three-dimensional view (size: 2.0 mm in length$\times$1.7 mm in width$\times$0.8 mm in height). (d) Plastic-embedded light microscopic section image (bar: 75 μm). Significantly fewer open tubule lumens are visible due to their occlusion with cytoplasmic debris (arrows). G: glomerulus.
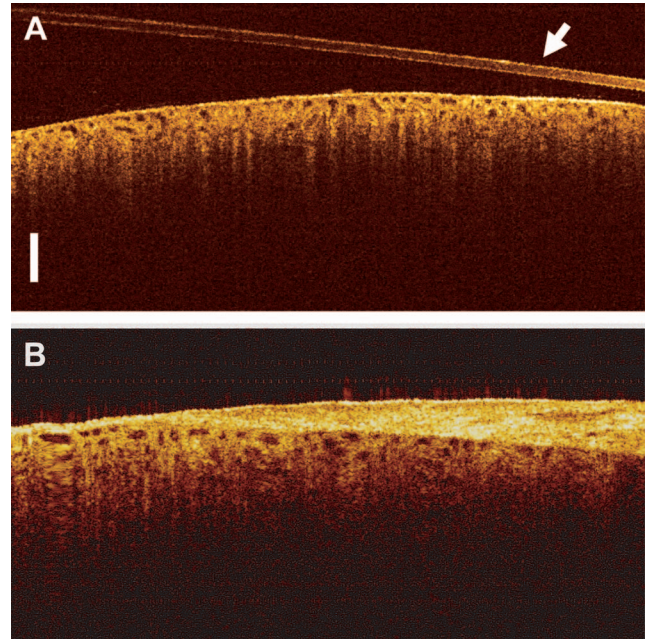

Fig. 7 Two-dimensional OCT axial images of kidneys surrounded by translucent plastic wrap (a) or covered with a layer of connective tissue (b). Note that, despite being within layers of plastic or connective tissue (arrows), the depth and quality of OCT images are unimpaired. Bars: 250 μm.
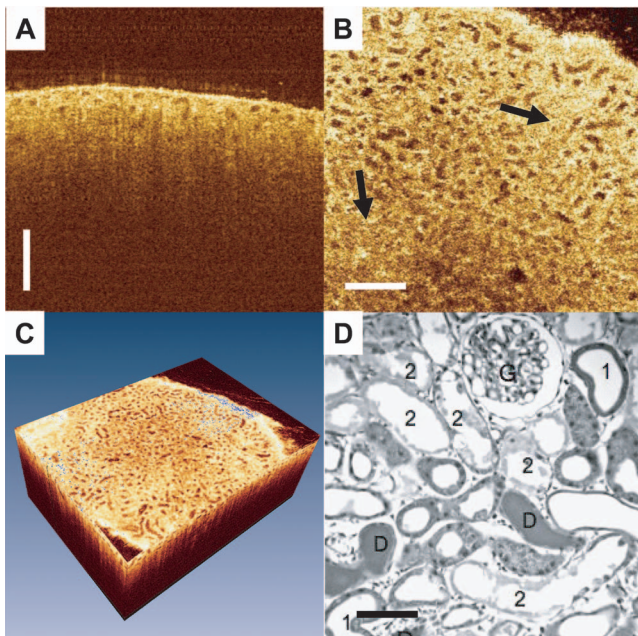

Fig. 6 OCT images of a kidney 48 h following infusion of mercuric chloride (1 mg/kg). (a) Cross-sectional image (bar: 250 μm). (b) *En face* image (bar: 250 μm). (c) Three-dimensional view (size: 2.1 mm in length$\times$1.6 mm in width$\times$0.8 mm in height). (d) Plastic-embedded light microscopic section image (bar: 100 μm). Although first-segment proximal tubules (1) appear normal, necrotic second-segment proximal tubules (2) and cast-filled distal tubules (D) appear as smudged areas in the OCT images (arrows). G: glomerulus.
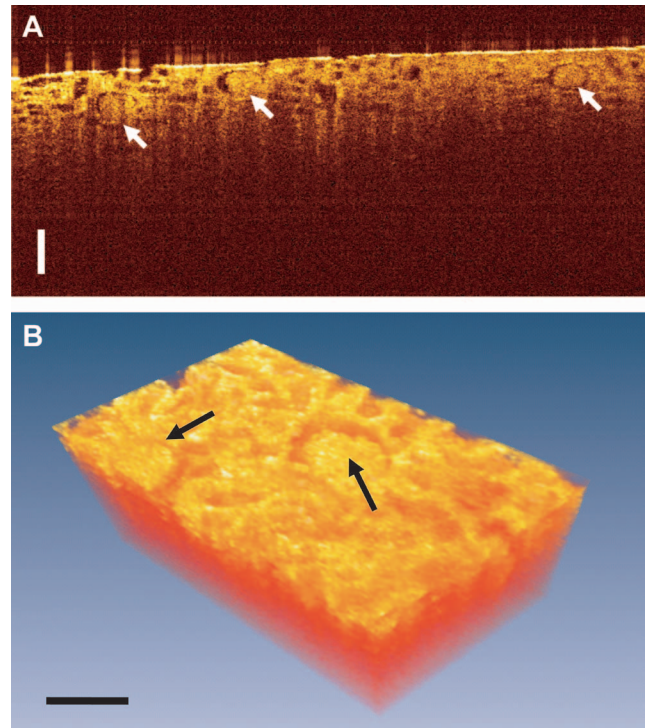

Fig. 8 (a) Cross-sectional OCT image revealing several glomeruli (arrows) subjacent to the surface of the kidney. Bar: 250 μm. (b) Three-dimensional reconstruction of OCT images seen in (a) reveals two glomeruli (arrows) and the surrounding capsular spaces of Bowman. Size: 1.7 mm (L)$\times$0.9 mm (W)$\times$1.0 mm (D). Bar: 100 μm.

will provide images characteristic of *in vivo* morphology and are not obtainable in excisional biopsies normally taken to analyze histopathology.[16] The latter underscores the need for a nonexcisional procedure to evaluate living kidneys.

The ischemic model of tubular necrosis reflects damage similar to that seen in kidneys being preserved prior to their transplantation. Specifically, cadaver kidneys destined for transplantation will undergo progressive tubular swelling and necrosis, thus resulting in tubular lumens filled with cytoplasmic debris.[19,20] Currently, transplant surgeons rely mainly on good preservation techniques and short preservation times to ensure donor kidney viability.[35] However, we recently reported that the degree of tubular necrosis seen in superficial proximal convoluted tubules can be used to predict the post-transplant function of kidneys.[17] Therefore, the ability to monitor such damage may be of considerable value in determining the status of donor kidneys. To address the circumstances of renal preservation, we evaluated the ability of OCT to image through translucent plastic bags and layers of fatty connective tissue, both of which can surround potential donor kidneys being preserved in cold conditions prior to their transplantation. We found that several layers of translucent plastic and a thin layer of connective tissue did not interfere with OCT imaging of the superficial uriniferous tubules, at least in the rat kidney. In human kidneys, however, the connective tissue capsule is of variable thickness and, in some cases, may be too thick to permit noninvasive imaging. In those cases, we believe that OCT imaging can be more easily performed using a sterile OCT catheter/needle inserted under the renal capsule. If OCT can be used to determine post-transplant renal function by providing immediate histopathological images, then OCT can be used to eliminate poor donor kidneys, as well as make available more donor kidneys that might otherwise be discarded due to long storage times or because of unknown ischemic damage (i.e., from non-heart-beating cadavers). Other forms of vital microscopy, including tandem scanning confocal microscopy[17] and near-infrared reflectance confocal microscopy,[36] have been recently used to image the kidney. However, their limited image penetration, combined with their traditional objectives and stages, make it difficult to evaluate human kidneys. OCT, on the other hand, not only permits deeper image penetration, but it also has the advantages of longer probe working distance and noncontact imaging. Furthermore, OCT can be performed with a small, sterile catheter or needle probe for minimally invasive *in vivo* imaging in the future.

In addition to studying the uriniferous tubules, we were able to successfully image intact renal corpuscles. Again, 3-D reconstructions of OCT images provided views of the renal corpuscles that are rivaled only by images obtained by scanning electron microscopy.[27] These images allowed us to evaluate glomerular size and shape, as well as the space between the glomerulus and the parietal epithelial capsule. Already, good correlations have been shown between glomerular size and such renal diseases as mesangial proliferative glomerulonephritis,[37] focal segmental glomerulosclerosis,[38] Type I diabetes mellitus,[39] and renal ischemia.[40] In addition to surface glomeruli, OCT can be used with catheters or needles to image glomeruli located deep in the cortex. A small, 27-gauge (410-μm diam) OCT imaging needle has already been demonstrated.[25] Unlike traditional renal needle biopsies that

are a blind procedure, OCT imaging needles could potentially provide immediate image information about all kidney glomeruli in the vicinity of the area being probed. Exactly how useful OCT will be in providing images that might help interpret the glomerular pathology awaits future studies.

References

1. D. Huang, E. A. Swanson, C. P. Lin, et al., "Optical coherence tomography," *Science* **254**, 1178–1181 (1991).
2. W. Drexler, U. Morgner, R. K. Ghanta, F. X. Kartner, J. S. Schuman, and J. G. Fujimoto, "Ultrahigh-resolution ophthalmic optical coherence tomography," *Nat. Med.* **7**, 502–507 (2001).
3. M. E. Brezinski, G. J. Tearney, N. J. Weissman, et al., "Assessing atherosclerotic plaque morphology: comparison of optical coherence tomography and high frequency intravascular ultrasound," *Heart* **77**, 397–403 (1997).
4. M. R. Hee, J. A. Izatt, E. A. Swanson, D. Huang, J. S. Schuman, C. P. Lin, C. A. Puliafito, and J. G. Fujimoto, "Optical coherence tomography of the human retina," *Arch. Ophthalmol. (Chicago)* **113**, 325–332 (1995).
5. C. A. Puliafito, M. R. Hee, C. P. Lin, et al., "Imaging of macular diseases with optical coherence tomography," *Ophthalmology* **102**, 217–229 (1995).
6. J. S. Schuman, C. A. Puliafito, and J. G. Fujimoto, *Optical Coherence Tomography of Ocular Diseases*, 2nd ed., Slack, Thorofare, NJ (2004).
7. J. G. Fujimoto, S. A. Boppart, G. J. Tearney, B. E. Bouma, C. Pitris, and M. E. Brezinski, "High resolution *in vivo* intra-arterial imaging with optical coherence tomography," *Heart* **82**, 128–133 (1999).
8. I. K. Jang, B. E. Bouma, D. H. Kang, et al., "Visualization of coronary atherosclerotic plaques in patients using optical coherence tomography: comparison with intravascular ultrasound," *J. Am. Coll. Cardiol.* **39**, 604–609 (2002).
9. B. E. Bouma, G. J. Tearney, C. C. Compton, and N. S. Nishioka, "High-resolution imaging of the human esophagus and stomach *in vivo* using optical coherence tomography," *Gastrointest. Endosc.* **51**, 467–474 (2000).
10. M. V. Sivak, K. Kobayashi, J. A. Izatt, et al., "High-resolution endoscopic imaging of the GI tract using optical coherence tomography," *Gastrointest. Endosc.* **51**, 474–479 (2001).
11. X. D. Li, S. A. Boppart, J. Van Dam, et al., "Optical coherence tomography: advanced technology for the endoscopic imaging of Barrett's esophagus," *Endoscopy* **32**, 921–930 (2000).
12. J. Welzel, E. Lankenau, R. Birngruber, and R. Engelhard, "Optical coherence tomography of the human skin," *J. Am. Acad. Dermatol.* **37**, 958–963 (1997).
13. L. L. Otis, M. J. Everett, U. S. Sathyam, and B. W. Colston, "Optical coherence tomography: a new imaging technology for dentistry," *J. Am. Dent. Assoc.* **131**, 511–514 (2000).
14. A. V. D'Amico, M. Weinstein, X. D. Li, J. P. Richie, and J. G. Fujimoto, "Optical coherence tomography as a method for identifying benign and malignant microscopic structures in the prostate gland," *Urology* **55**, 783–787 (2000).
15. C. Pitris, A. Goodman, S. A. Boppart, J. J. Libus, J. G. Fujimoto, and M. E. Brezinski, "High-resolution imaging of gynecologic neoplasms using optical coherence tomography," *Obstet. Gynecol. (N.Y., NY, U.S.)* **93**, 135–139 (1999).

16. A. B. Maunsbach, "The influence of different fixatives and fixation methods on the ultrastructure of rat kidney proximal tubule cells. I. Comparison of different perfusion fixation methods and of glutaraldehyde, formaldehyde, and osmium tetroxide fixatives," *J. Ultrastruct. Res.* **15**, 242–282 (1966).

17. P. M. Andrews, B. S. Khirabadi, and B. C. Bengs, "Using tandem scanning confocal microscopy (TSCM) to predict the status of donor kidneys," *Nephron* **91**, 148–155 (1983).

18. P. R. Herz, Y. Chen, A. D. Aguirre, et al., "Ultrahigh resolution optical biopsy with endoscopic optical coherence tomography," *Opt. Express* **12**, 3532–3542 (2004).

19. P. M. Andrews and A. K. Coffey, "Protection of kidneys from acute-renal failure resulting from normothermic ischemia," *Lab. Invest.* **49**, 87–98 (1983).

20. P. M. Andrews and A. K. Coffey, "Factors which improve the preservation of nephron morphology during cold storage," *Lab. Invest.* **46**, 100–120 (1982).

21. P. M. Andrews and A. K. Coffey, "A technique to reduce fixation artifacts to kidney proximal tubules," *Kidney Int.* **25**, 964–968 (1984).

22. P. M. Andrews and E. M. Chung, "High dietary protein regimens provide significant protection from mercury nephrotoxicity in rats," *Toxicol. Appl. Pharmacol.* **105**, 288–304 (1990).

23. J. G. Fujimoto, "Optical coherence tomography for ultrahigh resolution *in vivo* imaging," *Nat. Biotechnol.* **21**, 1361–1367 (2003).

24. A. G. Podoleanu, "Optical coherence tomography," *Br. J. Radiol.* **78**, 976–988 (2005).

25. X. Li, C. Chudoba, T. Ko, C. Pitris, and J. G. Fujimoto, "Imaging needle for optical coherence tomography," *Opt. Lett.* **25**, 1520–1522 (2000).

26. S. A. Boppart, J. Herrmann, C. Pitris, D. L. Stamper, M. E. Brezinski, and J. G. Fujimoto, "High-resolution optical coherence tomography-guided laser ablation of surgical tissue," *J. Surg. Res.* **82**, 275–284 (1999).

27. P. M. Andrews and K. R. Porter, "A scanning electron microscopic study of the nephron," *Am. J. Anat.* **140**, 81–116 (1974).

28. N. A. Nassif, B. Cense, B. H. Park, et al., "*In vivo* high-resolution video-rate spectral-domain optical coherence tomography of the human retina and optic nerve," *Opt. Express* **12**, 367–376 (2004).

29. R. A. Leitgeb, W. Drexler, A. Unterhuber, B. Hermann, T. Bajraszewski, T. Le, A. Stingl, and A. F. Fercher, "Ultrahigh resolution Fourier domain optical coherence tomography," *Opt. Express* **12**, 2156–2165 (2004).

30. M. Wojtkowski, V. J. Srinivasan, T. H. Ko, J. G. Fujimoto, A. Kowalczyk, and J. S. Duker, "Ultrahigh-resolution, high-speed, Fourier domain optical coherence tomography and methods for dispersion compensation," *Opt. Express* **12**, 2404–2422 (2004).

31. R. Huber, M. Wojtkowski, J. G. Fujimoto, J. Y. Jiang and A. E. Cable, "Three-dimensional and C-mode OCT imaging with a compact, frequency swept laser source at 1300 nm," *Opt. Express* **13**, 10523–10538 (2005).

32. A. Jain, A. Kopa, Y. T. Pan, G. K. Fedder, and H. K. Xie, "A two-axis electrothermal micromirror for endoscopic optical coherence tomography," *IEEE J. Sel. Top. Quantum Electron.* **10**, 636–642 (2004).

33. X. Liu, M. J. Cobb, Y. Chen, M. B. Kimmey, and X. D. Li, "Rapid-scanning forward imaging miniature endoscope for real-time optical coherence tomography," *Opt. Lett.* **29**, 1763–1765 (2004).

34. J. T. W. Yeow, V. X. D. Yang, A. Chahwan, M. L. Gordon, B. Qi, I. A. Vitkin, B. C. Wilson, and A. A. Goldenberg, "Micromachined 2-D scanner for 3-D optical coherence tomography," *Sens. Actuators, A* **117**, 331–340 (2005).

35. J. Light, "Viability testing in the non-heart-beating donor," *Transplant. Proc.* **32**, 179–181 (2000).

36. V. Campo-Ruiz, G. Y. Lauwers, R. R. Anderson, E. Delgado-Baeza, and S. Gonzalez, "Novel virtual biopsy of the kidney with near infrared reflectance confocal microscopy: a pilot study *in vivo* and *ex vivo*," *J. Urol. (Baltimore)* **175**, 327–336 (2006).

37. S. Daiman and I. Koni, "Glomerular enlargement in the progression of mesangial proliferative glomerulonephritis," *Clin. Nephrol.* **49**, 145–152 (1998).

38. E. Nyberg, S.-O. Bohmn, and U. Berg, "Glomerular volume and renal function in children with different types of nephrotic syndrome," *Pediatr. Nephrol.* **8**, 285–289 (1994).

39. H. J. Gunderson and R. Osterby, "Glomerular size and structure in diabetes mellitus II. Late abnormalities," *Disbetologia* **13**, 43–48 (1977).

40. K. Moran, J. Mulhall, D. Kelly, S. Sheehan, J. Dowsett, P. Dervan, and J. M. Fitzpatrick, "Morphological changes and alterations in regional intrarenal blood flow induced by graded renal ischemia," *J. Urol. (Baltimore)* **148**, 463–466 (1992).